Experimental section

Materials: All chemicals and solvents were commercially available and were used without further purification. DSPE-PEG 2000 was purchased from Shanghai yuanye biotechnology co., Ltd. Fetal bovine serum (FBS) and DMEM 4.5 % culture medium were commercially available from Sigma-Aldrich. Solvents were purified according to standard laboratory methods.

***Atmospheric pressure measurement*:** NMR of benzothiadiazole derivatives were recorded on a Brüker AM500 spectrometer using Tetramethyl silane (TMS, δ=0 ppm) as internal standard. The time-resolved PL decay spectra of the samples were also performed on an Edinburgh FLS980 fluorescence spectrometer at room temperature. Fluorescence spectra were carried out on a FS5 Spectrofluorometer (Edinburgh, England). The digital photo-graphs were captured by the 550D digital cameras (Canon, Japan). Absolute PL quantum yields (**PLQYs**) were determined with a spectrometer C11347 (Hamamatsu, Japan). Powder X-ray diffraction experiments were measured on a Philips X'Pert Pro diffractometer (Netherlands). Measurements were made in a 2θ range of 5-50° at room temperature with a step of 0.02° (2θ).The scan speed was 2 degree/min. Dynamic light scattering (DLS) measurements were performed using a Brookhaven BI-ZR5 instrument at room temperature. UV-vis spectra were recorded on a Shimadzu UV-2600 spectrophotometer (Japan). All in vivo experiments were performed in compliance with SPF (Tianjin) Biotechnology Co.,Ltd., LTD Animal Study Committee's requirements for the care and use of laboratory animals in research. BALB/c mice (average body weight of 15 g) from SPF (Tianjin) Biotechnology Co.,Ltd., were used for animal imaging studies.

High-pressure measurements: A piece of crystal was placed in the hole of a T301 steel gasket with a mixture of methanol and ethanol (V/V, 4/1) for pressure transmission medium (PTM) and ruby chip as pressure calibration. *In-situ* PL spectra at high pressure were accomplished on an Ocean Optics QE65000 pectrometer in the reflection mode. The 355 nm line of a DPSS laser(violet diode laser) with a spot size of 20 mm and a power of 10 *m*w was used as the excitation source. The diamond anvil cell (DAC) containing the sample was put on a Nikon fluorescence microscope to

focus the laser on the sample. PL photographs of the compressed **BTA-TPA** crystals were taken by an imaging camera (Canon EOS 5D Mark II) equipped on the fluorescence microscope. The camera can record the photographs under same conditions including the exposure time and intensity. *In-situ* absorption spectra were measured on Ocean Optics QE65000 spectro-photometer. *In-situ* IR micro-spectroscopy of crystalline powders at high pressure was performed on a Bruker Vertex80 V FTIR with KBr as the PTM.

Theoretical calculations: The equilibrium geometries of ground state (S_0) and the lowest excited singlet state (S_1) were optimized at the level of (TD-DFT)M06-2X/6-31G(d, p). Subsequently, the excitation energy and natural transition orbitals (NTOs) were evaluated. All calculations were carried out using Gaussian 09 (version D.01).[1] To investigate the single-crystal structures of BTA-TPA at different hydrostatic pressures(Figure S12), we first optimized the atomic positions of the crystallographic structure of **BTA-TPA**, and its initial crystalline structure was obtained from the experimental measurements under the ambient pressure. The optimization of geometric structures was conducted by using the projector augmented wave (PAW) method[2] with the Perdew-Burke-Ernzerhof (PBE) exchange-correlation functional[3] including the dDsC dispersion correction[4] in Vienna Ab initio Simulation Package (VASP)[5]. The pressure of the optimized crystallographic structure was set to be ambient pressure (0 GPa). In order to obtain the crystalline structures for BTA-TPA under a specified external pressure, we compressed the volume of the BTA-TPA unit cell by scaling the lattice constants of *a*, *b*, and *c* in a unified random proportion. We then optimized their atomic positions and all lattice parameters. Throughout the calculations, the convergence criterion of the total energy was set to be 10^{-5} eV in the self-consistent field iteration. The cutoff energy for the plane-wave basis set was set to be 600 eV. The cutoff radius for pair interactions was set to be 50 Å. A *k*-mesh of 3 × 3×1 was used during the structural optimization. The single-point energy calculations were performed on a *k*-mesh of 6 × 6 × 1.

***Preparation of BTA-TPA NPs*:** A THF solution (1 *m*L) containing BTA-TPA (0.2 mg) and DSPE-PEG (1 mg) was injected slowly into water (10 *m*L) with

sonication. The suspension was then stirred at room temperature overnight to evaporate the organic solvent. After THF was evaporated, the solution was concentrated to 2 mL，then the solutions were filtered through 0.45 μm microfilter to collect the **BTA-TPA** NPs suspension.

***Characterizing the diameter distribution by DLS for BTA-TPA NPs*:** From the stock solution of **BTA-TPA** NPs aqueous solution, 500 μL aqueous solution of nanoparticles was added to a quartz dish containing 3 mL deionized water, and then measured in the setup of dynamic light scattering (DLS, Brookhaven BI-ZR5 instrument). The particle size distribution of DLS was obtained after three parallel tests.

***Cytotoxicity study*:** To determine the BTA-TPA NPs cytotoxicity, a MTT cell proliferation and cytotoxicity test was performed in 96-well plates. Hela cells were seeded at a density of 5 $\times 10^3$ cells per well and the cells were cultured for 12 h in culture medium (100 μL of medium per well). Then, the **BTA-TPA** NPs in PBS buffer were added into the cell culture media to a final NPs concentration of 0.38-100 μg/mL. After incubation for 24 h, the cells in the culture medium of 0.1 mL were treated with MTT solution (10 μL) to measure cell survival. The absorbance of the solution was monitored at 450 nm using a microplate reader (Thermo) after 4 h incubation. The cell viability in each well was calculated from the obtained values as a percentage of control wells. The results were presented as a mean and standard deviation obtained from six samples.

***Cell culture and imaging*:** Hela cells were cultured in culture medium (DMEM 4.5%) containing 10% FBS, 1% penicillin streptomycin, and incubated at 37 °C in a 5% CO_2 atmosphere. Cells were seeded onto 35 mm glass-bottom dishes and allowed to grow until a confluence of 40 %. Prior to experiments, the medium was removed and the adherent cells were washed twice with PBS buffer to remove the remnant growth medium. The **BTA-TPA** NPs were then added to the plates and final concentration of fluorophore in culture medium was 20 μM. The cell nuclei were stained with bis-Benzimide H 33342 trihydrochloride (Hoechst 33342). After incubation for 3 h, the cells were washed three times with PBS buffer, which were further washed twice with

PBS buffer and stained by Hoechst 33342 for 10 min. The stained cells were then washed three times with PBS buffer and washed once with MeOH then washed three times with PBS buffer used for bioimaging subsequently. Under a Leica confocal laser microscope system, **BTA-TPA** NPs was excited at 514 nm and the emission was collected above 570-730 nm. No background fluorescence of cells was detected under the setting condition.

***In vivo imaging studies*:** Every time before imaging, the mice were anaesthetized with isoflurane. To investigate the lymphatic imaging of BTA-TPA NPs in mice, samples (0.2 mg/mL in 10 *m*M PBS, 50 μL solutions per mouse) were intradermally injected into the right forepaw pad of mice. In vivo fluorescence imaging was performed immediately after sample injection using the IVIS Lumina II imaging system (Caliper Life Sciences Inc. iTheraMedical, Germany). The NIR image was obtained with the excitation source of 500 nm and Cy5.5 for emission (695-750 nm)**.**

Synthesis of BTA-TPA: The mixture of 7-(4-(diphenylamino)phenyl)benzo [c][1,2,5] thiadiazole-4-carbaldehyde (0.62 g, 1.52 mmol) and 2-(4-(diphenyl-amino)phenyl) acetonitrile (0.43 g, 1.50 mmol) in ethanol (HPLC, 30 ml) was stirred at the room temperature for 5 min. And then, a spot of NaOMe were added, and stirred for 12 h. The resulting dye (**BTA-TPA**) was filtered and repeatedly washed with EtOH solution to give red powders (0.76 g, 76.8%).

^{1}H NMR (400 MHz, $CDCl_3$), δ 8.69 (d, *J*=8 Hz, 1H), 8.42 (s, 1H), 7.92 (d, *J*=8.4 Hz, 2H), 7.81 (d, *J*=7.6 Hz, 1H), 7.66 (d, *J*=8.8 Hz, 2H), 7.31 (t, *J*=8.4 Hz, 8H), 7.21-7.07 (m, 16H);

^{13}C NMR (100 MHz, $CDCl_3$): δ= 155.1, 153.2, 149.2, 148.7, 147.3, 147.0, 135.1, 132.8, 130.1, 130.0, 129.5, 129.4, 127.6, 127.3, 127.1, 127.0, 125.3, 125.2, 125.1, 124.0, 123.6, 122.4, 122.3, 118.3, 112.2；

HRMS (ESI, m/z) Calculated for Ion formula $C_{45}H_{32}N_5S$ = 674.2373, found $[M+1]^+$ = 674.2367

Table S1. Crystal data and structure refinement of crystals **BTA-TPA**.

Samples	**BTA-TPA (CCDC: 1888552)**
Formula	$C_{45}H_{31}N_5S$
Mr	673.81
Temperature (K)	100
Crystal system	triclinic
Space group	P-1
Crystal size (mm)	0.1 × 0.08 × 0.06
a (Å)	7.8139(2)
b (Å)	9.9797(2)
c (Å)	21.6351(7)
α (°)	87.227(2)
β (°)	84.360(2)
γ (°)	86.871(2)
V(Å^3)	1674.87(8)
Z	2
D_{calc} (mg/m^3)	1.336
Theta Range (°)	4.110 - 67.075
F (000)	704
h, *k*, l_{max}	9, 11, 25
N_{ref}	5979
T_{min}, T_{max}	0.79404, 1.00000
Independent reflections	5862
Goodness-of-fit on F^2	1.125
R_{int}	0.0252
$R_1[I>2\sigma(I)]$	0.0713
$wR_2[I>2\sigma(I)]$	0.1886
R_1(all data)	0.0764
wR_2(all data)	0.0713
S	1.125

$R_1 = \Sigma||F_o| - |F_c||/\Sigma|F_o|$, $wR_2 = [\Sigma w(F_o^2 - F_c^2)^2/\Sigma w(F_o^2)^2]^{1/2}$

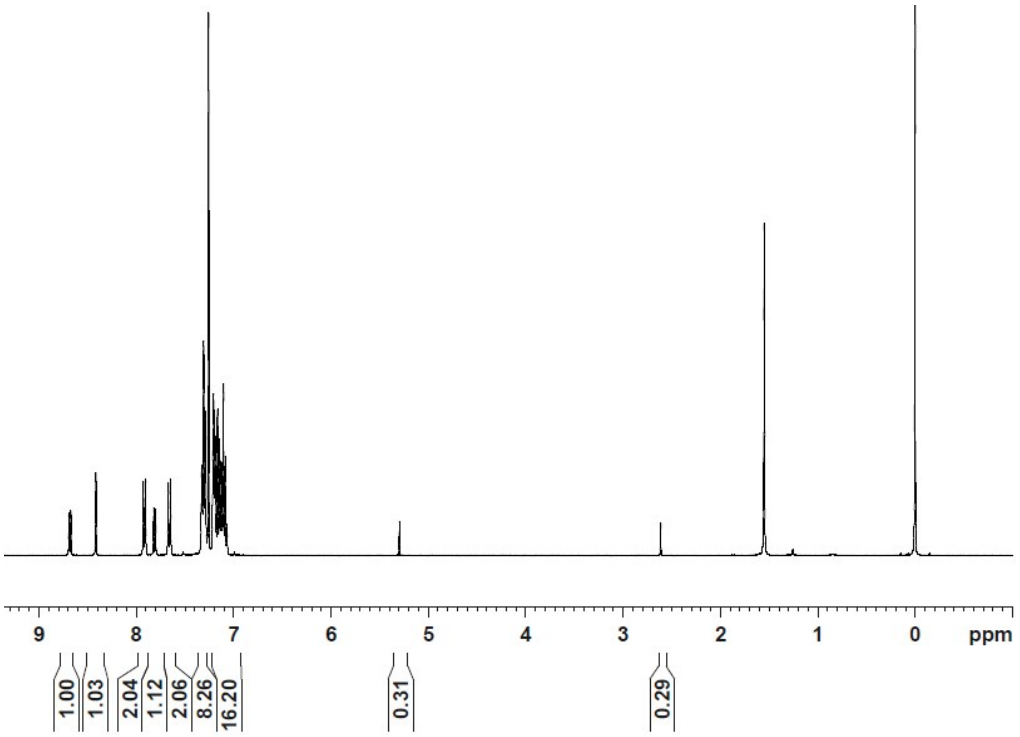

Fig. S1 ^{1}H-NMR spectra of **BTA-TPA**.

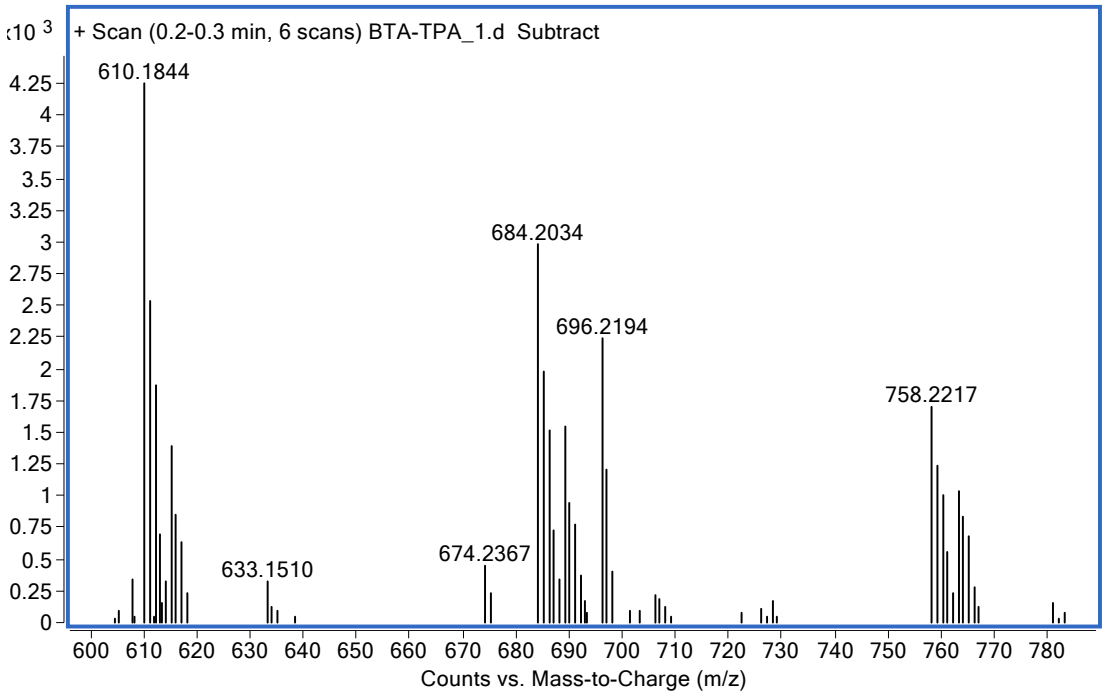

Formula (M)	Ion Formula	Calc m/z	m/z	Diff (ppm)
$C_{45}H_{31}N_5S$	$C_{45}H_{32}N_5S$	674.2373	674.2367	0.88

Fig. S2 The MS spectrum of **BTA-TPA**.

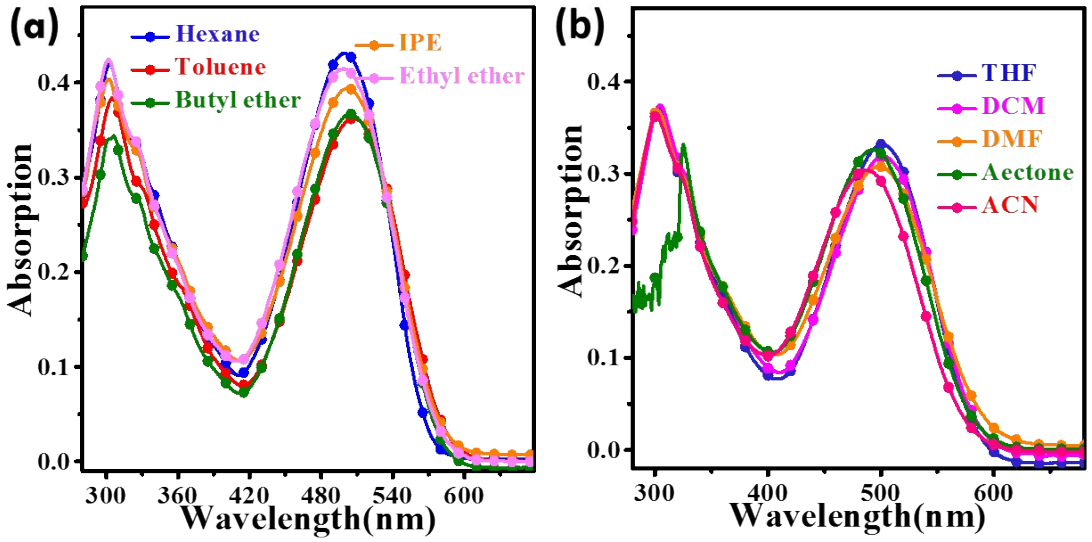

Fig. S3 The UV absorption spectra of **BTA-TPA**, measured in the different solvents with increasing polarity (the orientational polarizability of solvent, Δf, –hexane: 0.0012; toluene: 0.014; butyl ether: 0.096; isopropyl ether (IPE): 0.145; ethyl ether: 0.167; tetrahydrofuran (THF): 0.210; methylene chloride (DCM): 0.217; N,N-dimethylformamide (DMF): 0.276; Acetone: 0.284; and acetonitrile (ACN): 0.305).

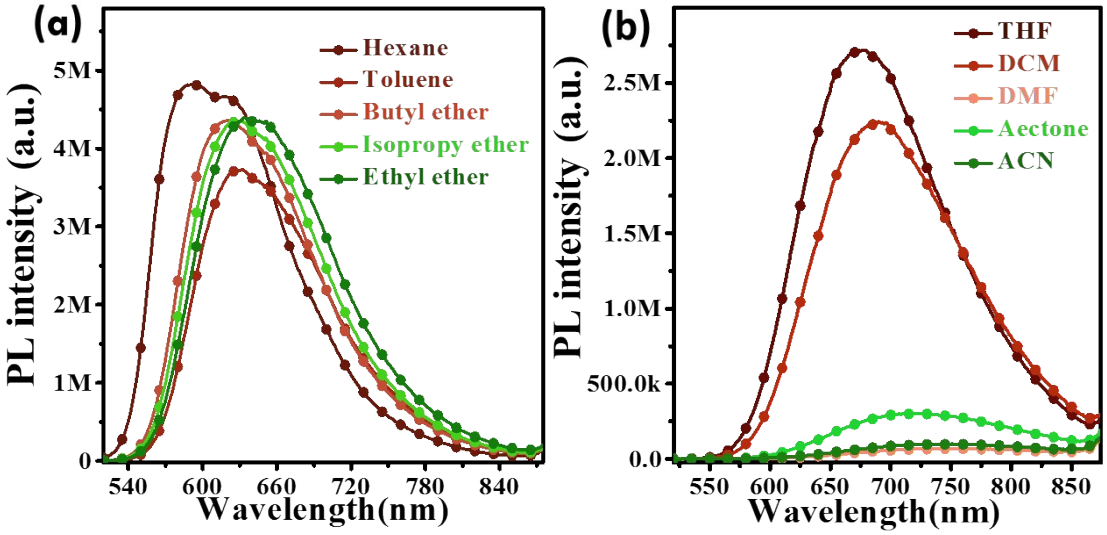

Fig. S4 Steady-state PL spectra of **BTA-TPA** in different solvents, the excitation wavelength is 500 nm.

The change in magnitude of the dipole moment between the ground and excited states, that is, $\Delta\mu = \lfloor \mu_e - \mu_g \rfloor$ can be estimated using the Lippert–Mataga equation

$$hc(\upsilon_a - \upsilon_f) = hc(\upsilon_a^0 - \upsilon_f^0) + \frac{2(\mu_e - \mu_e)^2}{a_0^3} f(\varepsilon,n)$$

Where a_0 is the cavity radius in which the solute resides, estimated to be 6.7 Å. μ_g is the ground-state dipole moment, estimated to be 2.25D (ωB97X at the basis set level of 6-31G**), μ_e is the excited state dipole moment. h and c are Planck's constant and the speed of light, respectively, and f(ε, n)is the orientation polarizability, defined as

$$f(\varepsilon,n) = \frac{\varepsilon - 1}{2\varepsilon + 1} - \frac{n^2 - 1}{2n^2 - 1}$$

Where ε is the static dielectric constant and n is the optical refractivity index of the solvent. Through the analysis of the fitted line in low-polarity solvents, its corresponding μ_e was calculated to be 7.6 D with the slope of 1627.7 (r^2= 0.6677) according to Lippert-Mataga equation. However, in high-polarity solvents, the μ_e was increased to 23.5D with the slope of 20913.9 (r^2= 0.9967).

Table S2 Detailed photo-physical data of **BTA-TPA** in the different solvents

Solvents	f	λ_{abs} nm	λ_{flu} nm	ν_a cm^{-1}	ν_f cm^{-1}	ν_a-ν_f cm^{-1}	Φ_{PL}
Hexane	0.0012	500	618	2.00×10^4	1.62×10^4	3.8×10^3	90.1%
Toluene	0.014	507	632	1.97×10^4	1.58×10^4	3.9×10^3	84.9%
Butyl ether	0.096	503	621	1.99×10^4	1.61×10^4	3.8×10^3	85.1%
Isopropyl ether	0.145	503	628	1.99×10^4	1.59×10^4	4.0×10^3	83.9%
Ethyl ether	0.167	499	633	2.00×10^4	1.58×10^4	4.2×10^3	82.4%
THF	0.210	503	679	1.99×10^4	1.47×10^4	5.2×10^3	62.5%
DCM	0.217	504	690	1.98×10^4	1.45×10^4	5.3×10^3	62.4%
DMF	0.276	501	758	2.00×10^4	1.32×10^4	6.8×10^3	2.8%
Acetonitrile	0.305	489	751	2.04×10^4	1.33×10^4	7.1×10^3	3.7%

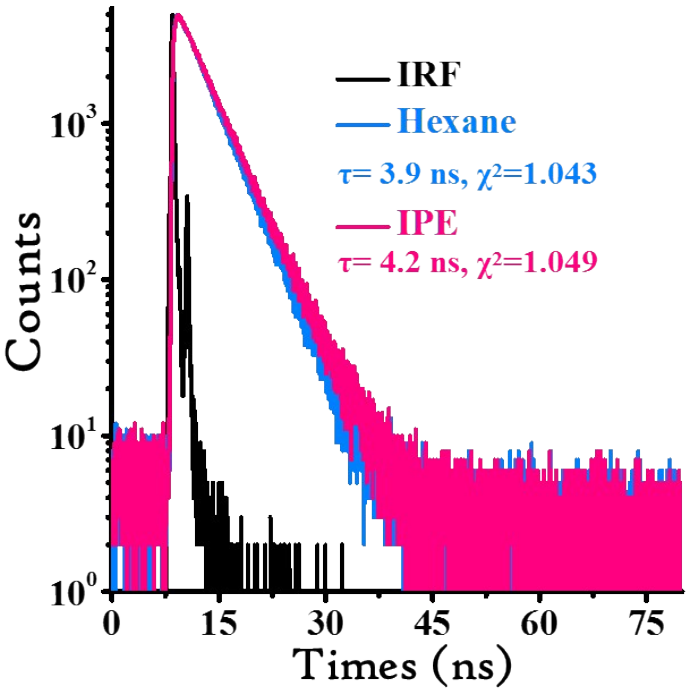

Fig. S5 The time-resolved PL lifetime of **BTA-TPA** in the hexane and IPE (10 μM), respectively.

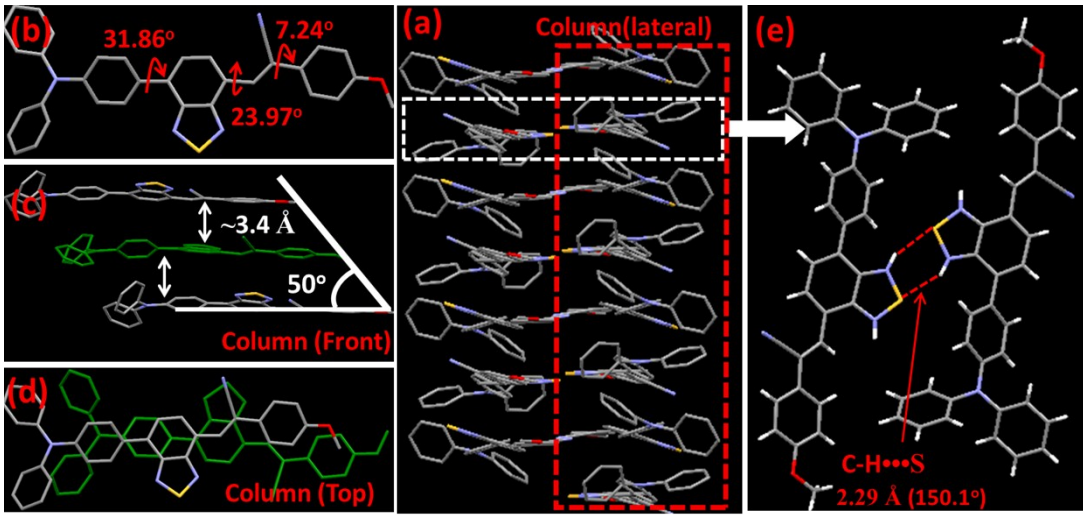

Fig. S6 Crystal structures of **BTA-MeO**: (*a*) Lateral view of the column arrangement; (*b*) the dihedral angles of the **BTA-MeO** single-crystal; (*c*) front view of the anti-parallel arrangement along long molecular axis (3.34 Å); (*d*) top view of the **BTA-MeO** dimer; (e) and illustration of the C–H•••S hydrogen bond interactions.

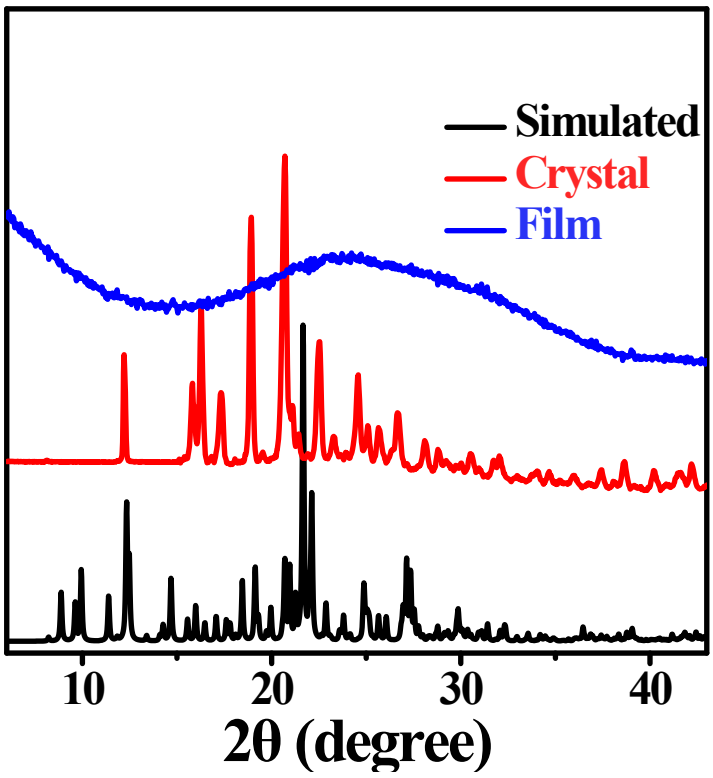

Fig. S7 XRD profiles of **BTA-TPA** in different states.

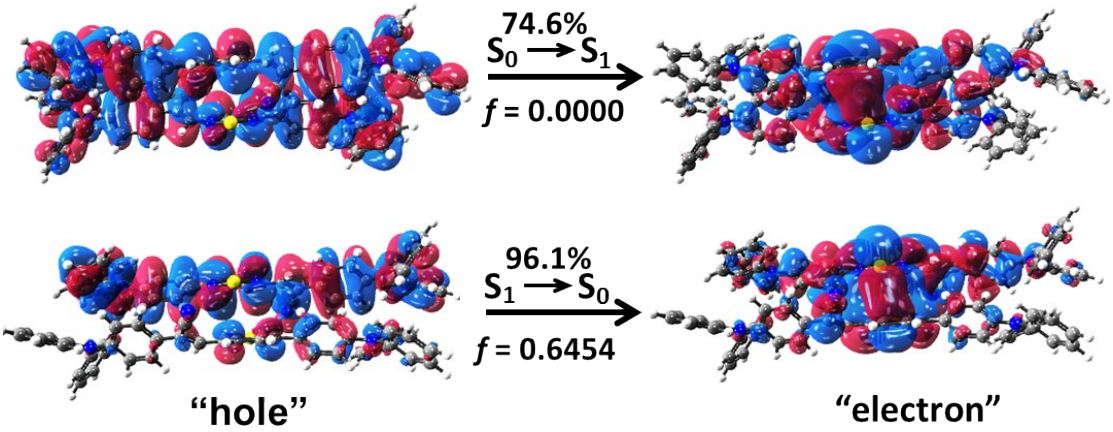

Fig. S8 Calculated NTOs of $S_1 \rightarrow S_0$ and $S_0 \rightarrow S_1$ for the **BTA-TPA** dimer based on S_1-geometry at the level of the TD/M06 -2X/6-31g(d,p), where *f* is the oscillator strength.

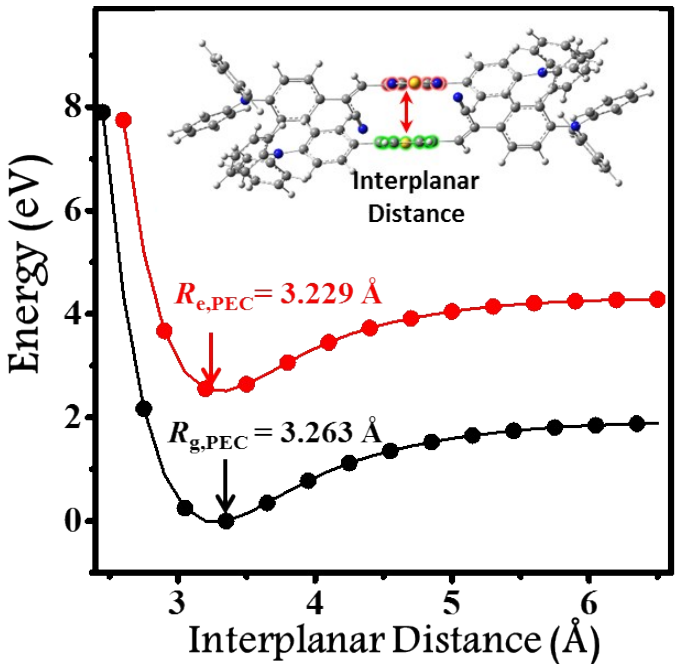

Fig. S9 Potential energy curves as a function of interplanar distance (R) of the dimer of **BTA-TPA** based on S_0 and S_1 states.

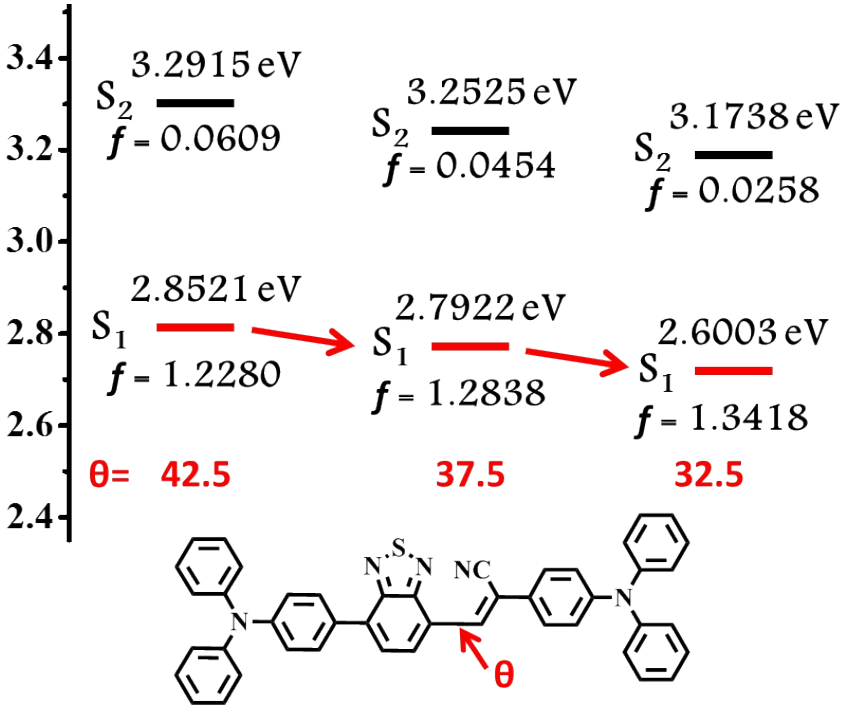

Fig. S10 The excitation energies (S_1 and S_2) of molecular conformation with the different torsion angles (θ), The calculations were carried out at the level of TD/M06-2X/6-31g(d,p), and *f* is the oscillator strength.

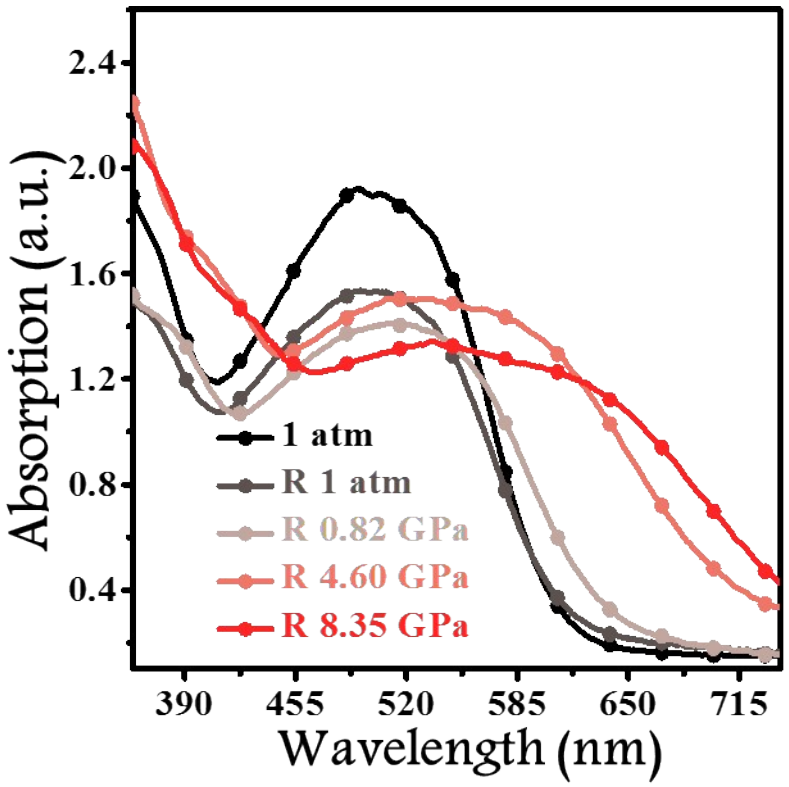

Fig. S11 Absorption spectrum of **BTA-TPA** crystal under different hydrostatic pressures during the depressurizing process.

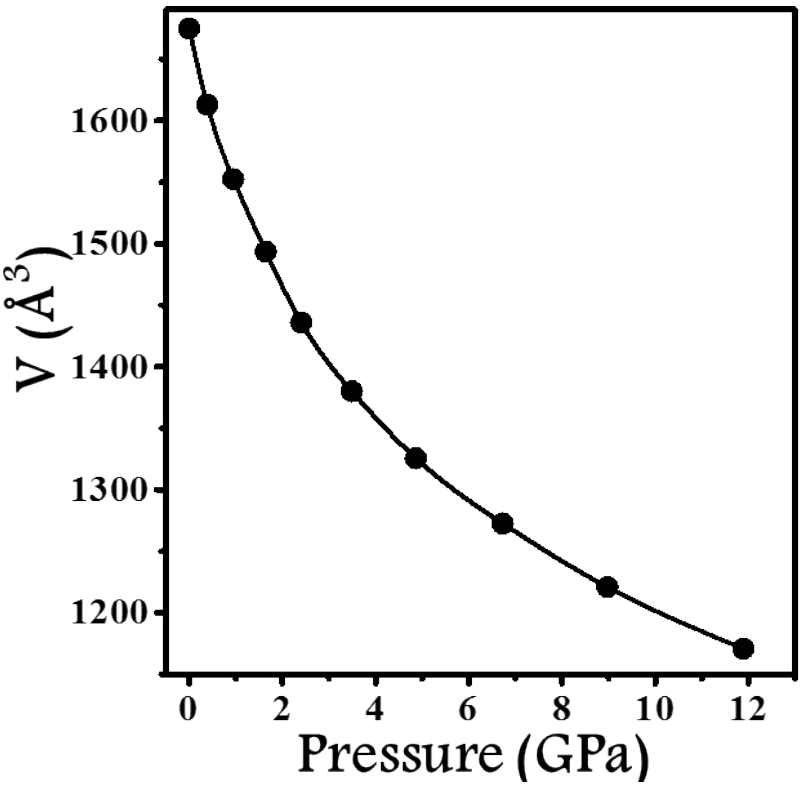

Fig. S12 Unit cell volume as a function of pressure.

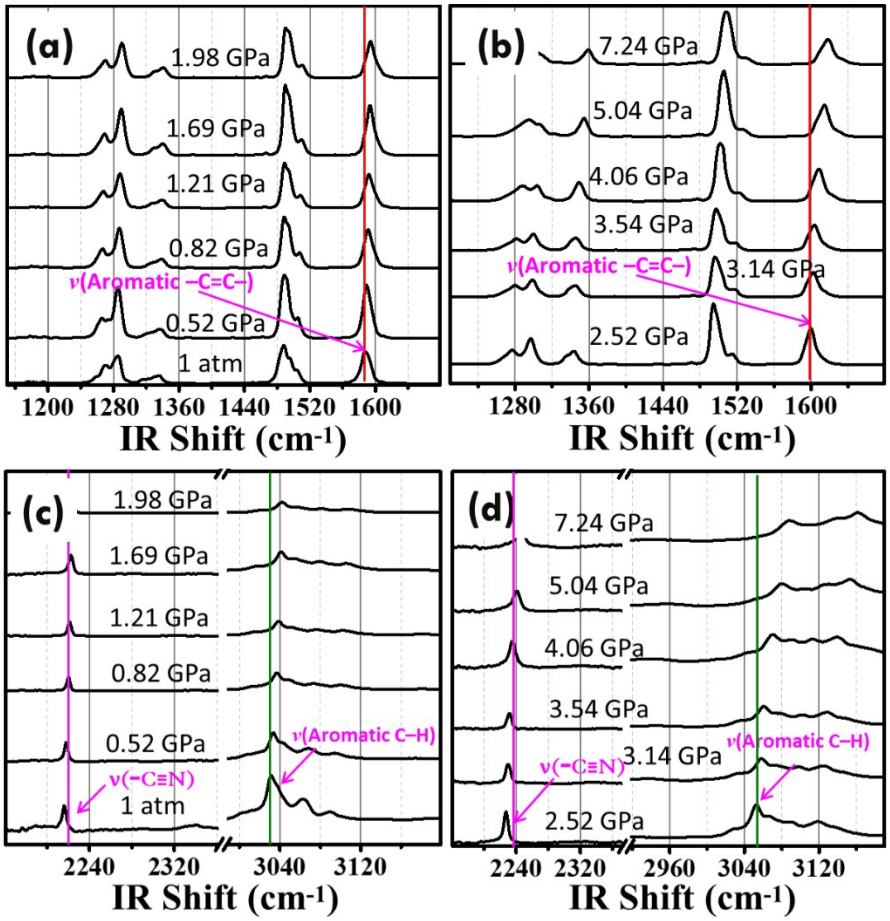

Fig. S13 IR spectra of **BTA-TPA** crystals in the range of 1000-3200 cm^{-1} at various pressures from 1 atm to 7.24 GPa.

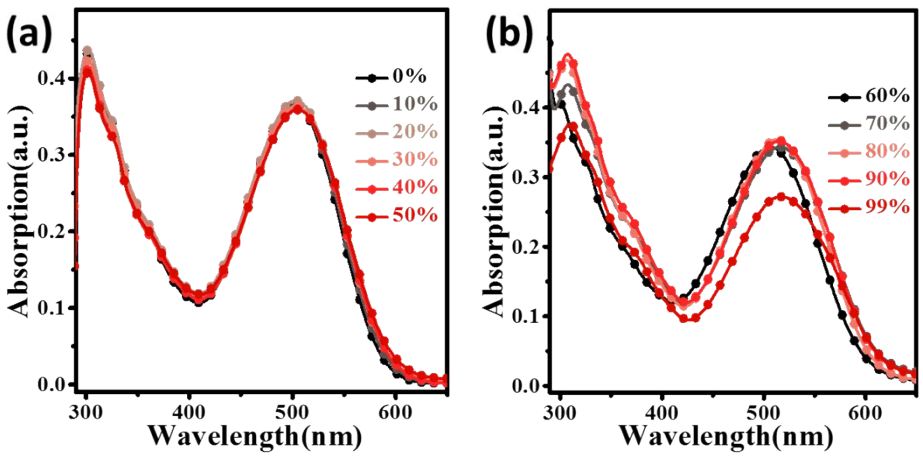

Fig. S14 (a) The UV absorption spectra of **BTA-TPA** (10 μM) in THF/water mixtures with different water fractions (f_w).

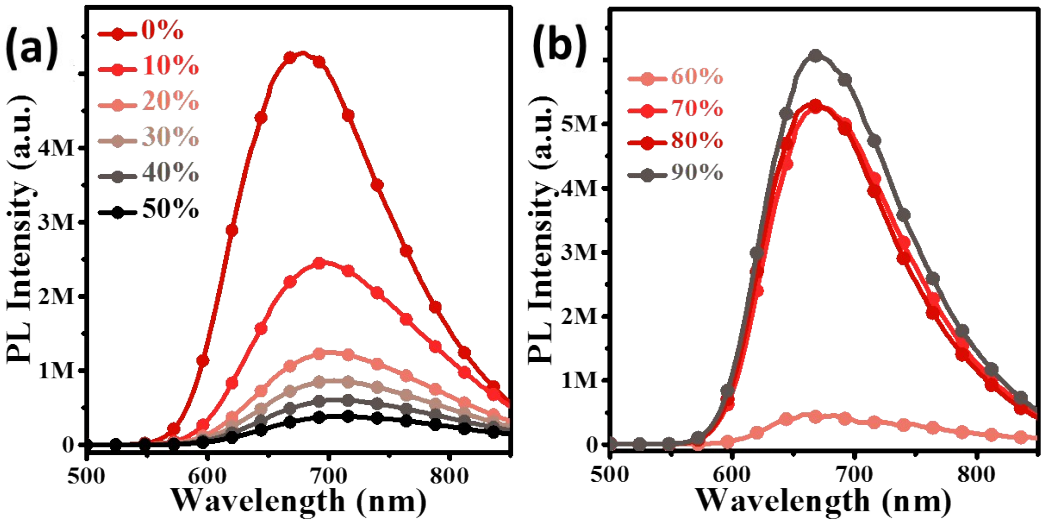

Fig. S15 (a) The PL spectra of **BTA-TPA** (10 μM) in THF/water mixtures with different water fractions (f_w).

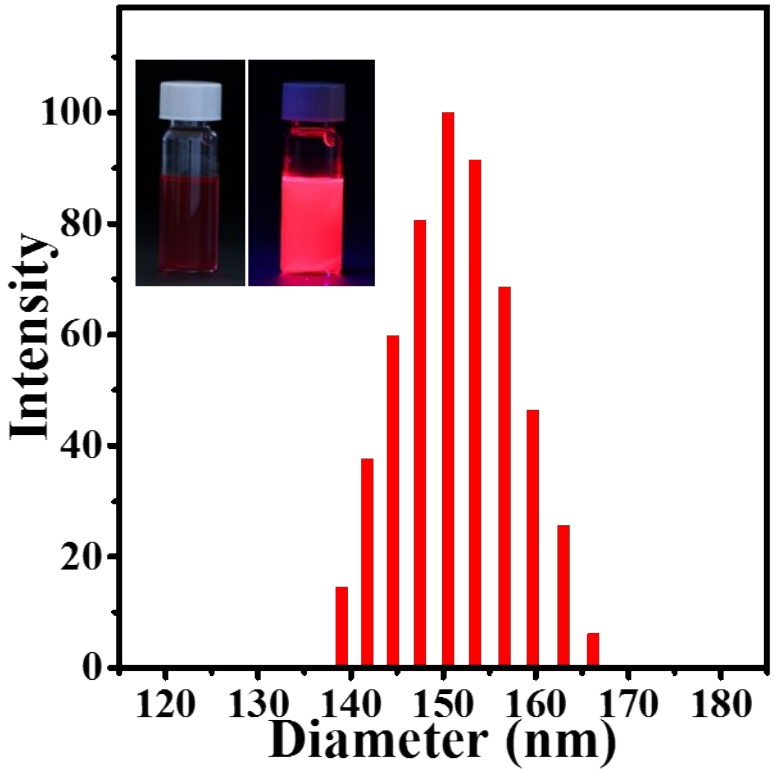

Fig. S16 Diameter of **BTA-TPA** NPs and picture of **BTA-TPA** NPs aqueous in day light and 365 nm light.

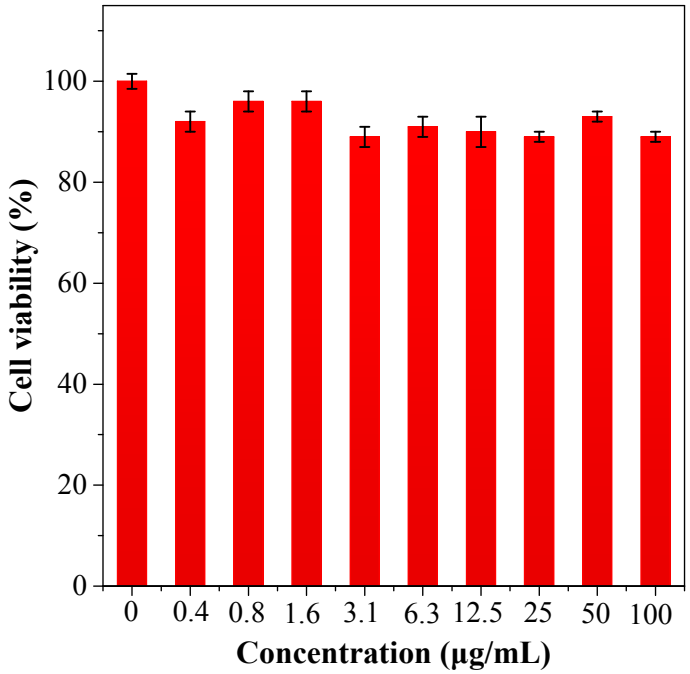

Fig. S17 Cytotoxicity of **BTA-TPA** NPs to Hela cells. Cellular internalization time is 12 hours at 37 °C

References

1 Frisch, M. J.; Trucks, G. W.; Schlegel, H. B.; Scuseria, G. E.; Robb, M. A.; Cheeseman, J. R.; Scalmani, G.; Barone, V.; Mennucci, B.; Petersson, G. A.; Nakatsuji, H.; Caricato, M.; Li, X.; Hratchian, H. P.; Izmaylov, A. F.; Bloino, J.; Zheng, G.; Sonnenberg, J. L.; Hada, M.; Ehara, M.; Toyota, K.; Fukuda, R.; Hasegawa, J.; Ishida, M.; Nakajima, T.; Honda, Y.; Kitao, O.; Nakai, H.; Vreven, T.; Montgomery Jr., J. A.; Peralta, J. E.; Ogliaro, F.; Bearpark, M. J.; Heyd, J.; Brothers, E. N.; Kudin, K. N.; Staroverov, V. N.; Kobayashi, R.; Normand, J.; Raghavachari, K.; Rendell, A. P.; Burant, J. C.; Iyengar, S. S.; Tomasi, J.; Cossi, M.; Rega, N.; Millam, N. J.; Klene, M.; Knox, J. E.; Cross, J. B.; Bakken, V.; Adamo, C.; Jaramillo, J.; Gomperts, R.; Stratmann, R. E.; Yazyev, O.; Austin, A. J.; Cammi, R.; Pomelli, C.; Ochterski, J. W.; Martin, R. L.; Morokuma, K.; Zakrzewski, V. G.; Voth, G. A.; Salvador, P.; Dannenberg, J. J.; Dapprich, S.; Daniels, A. D.; Farkas; Foresman, J. B.; Ortiz, J. V.; Cioslowski, J.; Fox, D. J.; Gaussian 09, Revision D.01; Gaussian, Inc.: Wallingford, CT, 2013.

2 P. E. Blöchl, Projector augmented-wave method. *Phys. Rev. B* 1994*,* **50**, 17953 - 17979.

3 J. P. Perdew, K. Burke, M. Ernzerhof, Generalized Gradient Approximation Made Simple. *Phys. Rev. Lett.* 1997, **78**, 1396-1396.

4 S. N. Steinmann, C. A Corminboeuf, Generalized-gradient approximation exchange hole model for dispersion coefficients. *J. Chem. Phys*. 2011, **134**, 044117.

5 G. Kresse, J. Furthmüller, Efficiency of ab-initio total energy calculations for metals and semiconductors using a plane-wave basis set. *Comput. Mater. Sci*. 1996, **6**, 15-50

6 Grimme, S. *J. Comput. Chem.* 2006, **27**, 1787.